Oxygen Transport Ceramic Membranes

Quarterly Report

April 2004 – June 2004

Principal Authors:
Prof. S. Bandopadhyay
Dr. N. Nagabhushana

Issued: May 2004

DOE Award # DE-FC26-99FT40054

School of Mineral Engineering,
University of Alaska Fairbanks
Fairbanks, AK 99775

Contributing sub contractors:

1. **X.-D Zhou, Q. Cai, J. Yang, W. B. Yelon, W. J. James and H. U. Anderson,** Materials Research Center, University of Missouri-Rolla, Rolla, MO 65401

2. **Prof. Alan Jacobson and Prof. C.A. Mims;** University of Houston/University of Toronto

DISCLAIMER

ABSTRACT

The present quarterly report describes some of the investigations on the structural properties of dense OTM bars provided by Praxair and studies on newer composition of Ti doped LSF.

In this report, *in situ* neutron diffraction was used to characterize the chemical and structural properties of $La_{0.2}Sr_{0.8}Fe_{0.55}Ti_{0.45}O_{3-\delta}$ (here after as L2SF55T) specimen, which was subject to measurements of neutron diffraction from room temperature to 900ºC in N_2. Space group of R3c was found to result in a better refinement and is used in this study. The difference for crystal structure, lattice parameters and local crystal chemistry for LSFT nearly unchanged when gas environment switched from air to N_2.

Stable crack growth studies on Dense OTM bars provided by Praxair were done at room temperature in air. A bridge-compression fixture was fabricated to achieve stable pre-cracks from Vickers indents. Post fracture evaluation indicated stable crack growth from the indent and a regime of fast fracture. Post-fracture X-ray data of the OTM fractured at 1000ºC in environment were refined by FullProf code and results indicate a distortion of the parent cubic perovskite to orthorhombic structure with reduced symmetry. TGA-DTA studies on the post-fracture samples also indicated residual effect arising from the thermal and stress history of the samples.

The thermal and chemical expansion of $La_{0.2}Sr_{0.8}Fe_{0.55}Ti_{0.45}O_{3-\delta}$ were studied at $800 \leq T \leq 1000$ °C and at $\sim 1 \times 10^{-15} \leq pO_2 \leq 0.21$ atm. The thermal expansion coefficient of the sample was calculated from the dilatometric analysis in the temperature range between room temperature and 1200 °C in air. A series of isotope transients under air separation mode (small gradient) were completed on the membrane of LSCrF-2828 at 900°C. Low pO_2 atmospheres based on with CO - CO_2 mixtures have also been admitted to the delivery side of the LSCrF-2828 membrane to produce the gradients which exist under syngas generation conditions. The CO - CO_2 mixtures have normal isotopic ^{18}O abundances. The evolution of ^{18}O on the delivery side in these experiments after an ^{18}O pulse on the air side reveals a wealth of information about the oxygen transport processes

TABLE OF CONTENTS

LIST OF GRAPHICAL MATERIALS

INTRODUCTION

Conversion of natural gas to liquid fuels and chemicals is a major goal for the Nation as it enters the 21st Century. Technically robust and economically viable processes are needed to capture the value of the vast reserves of natural gas on Alaska's North Slope, and wean the Nation from dependence on foreign petroleum sources. Technologies that are emerging to fulfill this need are all based syngas as an intermediate. Syngas (a mixture of hydrogen and carbon monoxide) is a fundamental building block from which chemicals and fuels can be derived. Lower cost syngas translates directly into more cost-competitive fuels and chemicals.

The currently practiced commercial technology for making syngas is either steam methane reforming (SMR) or a two-step process involving cryogenic oxygen separation followed by natural gas partial oxidation (POX). These high-energy, capital-intensive processes do not always produce syngas at a cost that makes its derivatives competitive with current petroleum-based fuels and chemicals.

In the mid 80's BP invented a radically new technology concept that will have a major economic and energy efficiency impact on the conversion of natural gas to liquid fuels, hydrogen, and chemicals.[1] This technology, called Electropox, integrates oxygen separation with the oxidation and steam reforming of natural gas into a single process to produce syngas with an economic advantage of 30 to 50 percent over conventional technologies.[2]

The Electropox process uses novel and proprietary solid metal oxide ceramic oxygen transport membranes [OTMs], which selectively conduct both oxide ions and electrons through their lattice structure at elevated temperatures.[3] Under the influence of an oxygen partial pressure gradient, oxygen ions move through the dense, nonporous membrane lattice at high rates with

[1]Mazanec, T. J.; Cable, T. L.; Frye, J. G., Jr.; US 4,793,904, 27 Dec **1988**, assigned to The Standard Oil Company (now BP America), Mazanec, T. J.; Cable, T. L.; US 4,802,958, 7 Feb **1989**, assigned to the Standard Oil Co. (now BP America), Cable, T. L.; Mazanec, T. J.; Frye, J. G., Jr.; European Patent Application 0399833, 24 May **1990**, published 28 November **1990.**

[2]Bredesen, R.; Sogge, J.; "A Technical and Economic Assessment of Membrane Reactors for Hydrogen and Syngas Production" presented at Seminar on the Ecol. Applic. of Innovative Membrane Technology in the Chemical Industry", Cetraro, Calabria, Italy, 1-4 May **1996**.

[3]Mazanec, T.J., *Interface*, **1996**; Mazanec, T.J., *Solid State Ionics*, 70/71, **1994** 11-19; "Electropox: BP's Novel Oxidation Technology", T.J. Mazanec, pp 212-225, in "The Role of Oxygen in Improving Chemical Processes", M. Fetizon and W.J. Thomas, eds, Royal Society of Chemistry, London, **1993**; "Electropox: BP's Novel Oxidation Technology", T.J. Mazanec, pp 85-96, in "The Activation of Dioxygen and Homogeneous Catalytic Oxidation", D.H.R. Barton, A. E. Martell, D.T. Sawyer, eds, Plenum Press, New York, **1993**; "Electrocatalytic Cells for Chemical Reaction", T.J. Mazanec, T.L. Cable, J.G. Frye, Jr.; Prep Petrol Div ACS, San Fran, **1992** 37, 135-146; T.J. Mazanec, T.L. Cable, J.G. Frye, Jr.; *Solid State Ionics*, **1992**, 53-56, 111-118.

100 percent selectivity. Transported oxygen reacts with natural gas on the fuel side of the ceramic membrane in the presence of a catalyst to produce syngas.

In 1997 BP entered into an OTM Alliance with Praxair, Amoco, Statoil and Sasol to advance the Electropox technology in an industrially sponsored development program. These five companies have been joined by Phillips Petroleum and now are carrying out a multi-year $40+ million program to develop and commercialize the technology. The program targets materials, manufacturing and engineering development issues and culminates in the operation of semi-works and demonstration scale prototype units.

The Electropox process represents a truly revolutionary technology for conversion of natural gas to synthesis gas not only because it combines the three separate unit operations of oxygen separation, methane oxidation and methane steam reforming into a single step, but also because it employs a chemically active ceramic material in a fundamentally new way. On numerous fronts the commercialization of Electropox demands solutions to problems that have never before been accomplished. Basic problems in materials and catalysts, membrane fabrication, model development, and reactor engineering all need solutions to achieve commercial success.

Six important issues have been selected as needing understanding on a fundamental level at which the applied Alliance program cannot achieve the breadth and depth of understanding needed for rapid advancement. These issues include:

1. Oxygen diffusion kinetics (University of Houston);
2. Phase stability and stress development (University of Missouri - Rolla);
3. Mechanical property evaluation in thermal and chemical stress fields (University of Alaska Fairbanks)

Statement of Work

Task 1   *Evaluate phase stability and thermal expansion of candidate perovskite membranes and develop techniques to support these materials on porous metal structures.*

Task 2   *Determine materials mechanical properties under conditions of high temperatures and reactive atmospheres.*

Task 3   *Measure kinetics of oxygen uptake and transport in ceramic membrane materials under commercially relevant conditions using isotope labeling techniques.*

EXECUTIVE SUMMARY

Research on the Oxygen Transport Membranes as listed as tasks 1-3 are being performed at the various universities under the stewardship of Praxair. The quarterly technical report presents the progress of the tasks defined to understand the fundamental concepts and structural performance of the OTM material.

It is of interest to that unlike the LSF series, the changes of lattice parameters for LSFT in air and nitrogen are not obvious. Unit cell volume as a function of lattice parameter also indicates the similar behavior. The obvious answer seems to be the substitution of Ti into LSF. This still did not resolve the reason for Ti to stabilize the structure upon changing gas environments. Further work will be aimed at understanding this phenomenon by using thermogravemetric analysis and transport measurements.

Stable crack growth studies on Dense OTM bars provided by Praxair were done at room temperature in air. A bridge-compression fixture was fabricated to achieve stable pre-cracks from Vickers indents. Post fracture evaluation indicated stable crack growth from the indent and microscopic observation clearly indicated an indented region, a regime of slow and stable crack growth, fast fracture and compression curl in the tested sample. This result is indicative of a "good-test run" and since the method is very simple will also be used on samples to be tested in the environmental conditions (temp, pressure and chemical environment). Results from the refinement of XRD data indicate that the parent perovskite with a primitive cubic perovskite structure (a=b=c = 3.9104A°) undergoes a slight distortion to orthorhombic structure (Pmmm) with reduced crystal symmetry. Although slight changes are observed in the a axis, the distortion is primarily in the c and b axes. Interestingly, samples tested under stress and environment showed increasing distortion with decreasing stress rates. However, although the major peaks were refined, the broader reflections and splitting of several peaks indicate the possible presence of secondary phases etc. Further refinement of the data will be done considering various phase composition determined by XRD. TGA-DTA studies on the post-fracture samples also indicated residual effect arising from the thermal and stress history of the samples. The results indicate that there is a perceptible change in stoichiometry of the fractured OTM membrane as compared to related studies on non-fractured samples. However, based on the discussion with the group at the project meeting further tests such as removing the thermal and applied stress history by annealing are planned to confirm the results.

The thermodynamic properties (stability and phase-separation behavior) and total conductivity of prototype membrane materials were further investigated. The data are needed together with the kinetic information to develop a complete model for the membrane transport. Characterization, stoichiometry, conductivity, and dilatometry measurements for samples of La0.2Sr0.8Fe0.55Ti0.45O3-x has been previously reported. In this report, further measurements of the chemical and thermal expansion as a

function of temperature and pO2.are described. Continued analysis of LSCF-6428 quenched membrane with better resolution and signal/noise to retrieve isotope profiles from the SIMS data was carried out. Also, a series of isotope transients under air separation mode (small gradient) were completed on the membrane of LSCrF-2828 at 900°C. The reversibility of oxygen activation at the air side could be obtained by observing the exchange of oxygen from the solid into the air after the administration of the isotope labeled pulse.

Task 1:   Preparation and Characterization of Dense Ceramic oxygen Permeable Membranes

X.-D Zhou[1], Q. Cai[2], J. Yang[1], W. B. Yelon[1], W. J. James[1] and H. U. Anderson[1]

1.   **Materials Research Center, University of Missouri-Rolla, Rolla, MO 65401**
2.   **Department of Physics, University of Missouri-Columbia, Columbia, MO 65211**

In situ Neutron Diffraction Analysis of $La_{0.2}Sr_{0.8}Fe_{0.55}Ti_{0.45}O_{3-\delta}$ - N_2

Experimental

L2SF55T specimen was sintered at 1400ºC for 2 hours and then cooling to room temperature at 3ºC/min. The bar sample with a geometry ~35mmx3mmx3mm was hung in the high temperature furnace which was designed to conduct *in situ* neutron diffraction measurements in N_2. The neutron measurements were carried out using the position sensitive detector – diffractometer at the University of Missouri Research Reactor (MURR) in Columbia, MO.   For Neutron Diffraction (ND) studies, samples were contained in 3 mm V metal cells and data were collected at 1.4785 Å over a range of 5º-105º (2θ). Rietveld refinement was carried out using the FULLPROF code, in which the magnetic ordering was taken into account because of the sensitivity of neutron diffraction to the magnetic ordering of the Fe atoms.

Results and Discussion

Table 1 shows parameters refined from *in situ* neutron diffraction measurements of LSFT in air with space group of R3c. Refinement data of the sample measured in N_2 are listed in Table 2.

It is of interest to see how Fig. 1 and Fig. 2 illustrate plots of lattice parameters for LSFT in air and nitrogen. Unlike LSF series, changes of lattice parameters of LSFT are not obvious. Unit cell volume as a function of lattice parameter indicates the similar behavior (see Fig. 3).

Oxygen occupancy in air and N_2 is compared in Fig. 4 as a function of temperature. Again, the variation of these changes can be considered in the error bar of the measurements and refinements.

Now, the question remains as why there exists a significant difference between LSF and LSFT. The obvious answer is because of substituting Ti into LSF. This still did not resolve the reason for Ti to stabilize the structure upon changing gas environments. Future work will be aimed at understanding this phenomenon by using thermogravemetric analysis and transport measurements.

Table 1   Refined with r-3c and oxygen is at 36f only:

2nd run: occ(La)/Sr=0.033/0.133, Fe/Ti=0.09/0.077

Temp	a	c	x(o)	y(o)	z(o)	B(A)	B(B)	B(o)	Occ(o)	socc	Vol	svol	χ^2
RT	5.51886(43)	13.49961(216)	0.502(2)	0.014(3)	0.238(1)	1.96(5)	1.05(6)	1.7(1)	0.488	2	356.082	69	6.24
97	5.53433(25)	13.53199(121)	0.502(1)	0.014(2)	0.2374(7)	0.99(5)	0.63(8)	0.90(8)	0.498	3	358.941	39	3.10
198	5.54184(26)	13.55118(130)	0.505(3)	0.012(2)	0.2361(7)	1.18(6)	0.81(8)	0.90(9)	0.496	3	360.426	42	3.13
294	5.54958(26)	13.56964(129)	0.51(1)	0.015(2)	0.2371(7)	1.36(6)	0.99(8)	1.19(8)	0.497	3	361.926	42	2.92
401	5.55826(25)	13.58761(127)	0.510(2)	0.014(2)	0.2364(7)	1.45(6)	0.97(8)	1.17(9)	0.495	4	363.539	41	2.97
504	5.56681(27)	13.60917(139)	0.507(5)	0.013(2)	0.2357(7)	1.71(6)	1.31(9)	1.29(9)	0.494	4	365.237	45	2.93
598	5.57509(30)	13.63258(152)	0.511(2)	0.017(3)	0.2374(9)	1.68(6)	1.25(9)	1.54(9)	0.497	4	366.954	50	2.52
696	5.58472(35)	13.65723(179)	0.510(4)	0.017(3)	0.237(1)	1.84(7)	1.46(9)	1.8(1)	0.497	4	368.889	58	2.65
798	5.59583(34)	13.68131(178)	0.509(3)	0.015(2)	0.2354(9)	2.12(7)	1.8(1)	1.8(1)	0.491	4	371.012	58	2.80
891	5.60397(37)	13.70493(198)	0.51(3)	0.019(3)	0.236(1)	2.68(7)	2.2(1)	2.1(1)	0.478	3	372.734	64	2.41

Table 2. LSFT 1400C Bulk sample at high temperature, N2, r-3c, oxygen occupy 36f only, occ(La)/Sr=0.033/0.133, Fe/Ti=0.09/0.077

| Temp	a	c	x(o)	y(o)	z(o)	B(A)	B(B)	B(o)	Occ(o)	socc	Vol	svol	χ^2
RT	5.53051(23)	13.52257(116)	0.500(1)	0.010(1)	0.2358(6)	1.35(5)	1.12(7)	1.05(8)	0.485	3	358.196	37	6.04
100	5.53236(25)	13.52822(116)	0.501(2)	0.015(3)	0.2409(9)	1.01(5)	0.71(7)	1.24(7)	0.505	3	358.585	38	2.96
200	5.54202(23)	13.54731(110)	0.502(2)	0.010(2)	0.2378(7)	1.25(6)	0.90(8)	1.05(8)	0.497	3	360.347	36	3.23
296	5.54862(21)	13.56198(102)	0.503(2)	0.012(2)	0.2374(6)	1.36(6)	1.00(8)	1.15(8)	0.499	3	361.596	34	3.03
403	5.55676(24)	13.58362(117)	0.503(2)	0.012(2)	0.2370(7)	1.58(6)	1.21(8)	1.32(8)	0.504	4	363.236	38	3.05
503	5.56382(24)	13.60065(120)	0.503(2)	0.012(2)	0.2370(7)	1.74(6)	1.39(9)	1.51(9)	0.505	4	364.617	39	2.98
601	5.57105(26)	13.62131(124)	0.51(7)	0.016(3)	0.2394(8)	1.84(6)	1.46(8)	1.76(8)	0.495	3	366.120	41	2.42
698	5.58519(25)	13.65260(125)	0.504(2)	0.015(2)	0.2369(7)	2.11(7)	1.73(9)	1.81(9)	0.492	4	368.826	41	2.71
802	5.58909(27)	13.66213(132)	0.504(2)	0.017(3)	0.2373(8)	2.86(7)	2.33(9)	2.42(9)	0.484	3	369.599	43	2.68
893	5.59640(44)	13.69344(234)	0.512(6)	0.022(4)	0.237(1)	2.94(7)	2.6(1)	2.43(9)	0.478	3	371.416	76	2.44
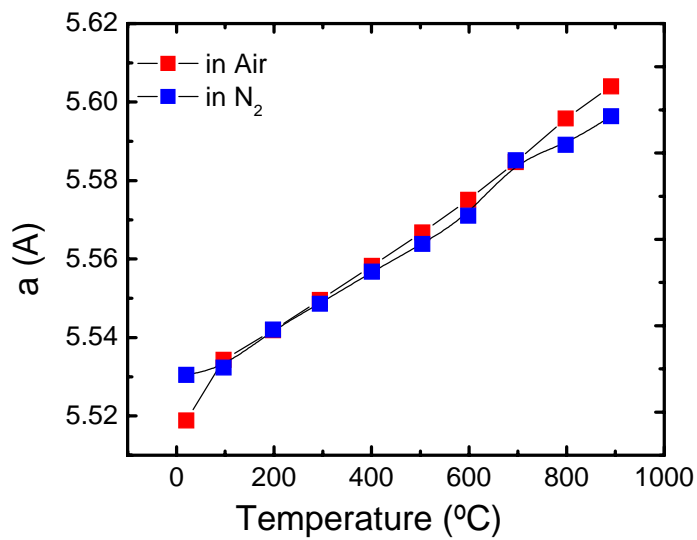
Fig. 1. Lattice parameter (a) as a function of temperature for LSFT in air and N_2.
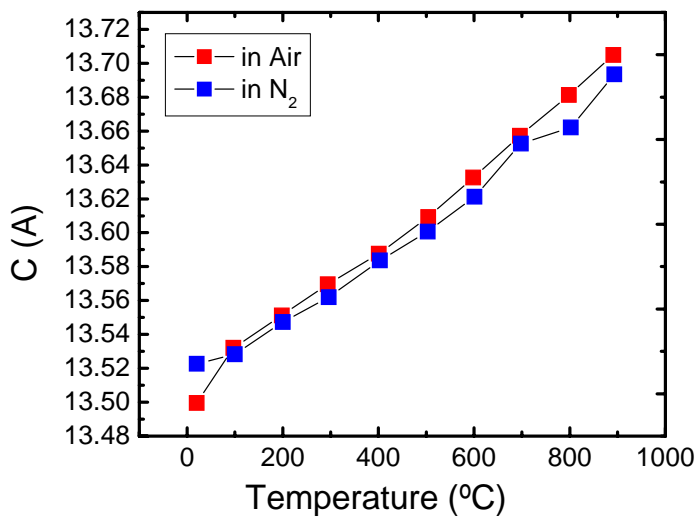

Fig. 2. Lattice parameter (c) as a function of temperature for LSFT in air and N_2.
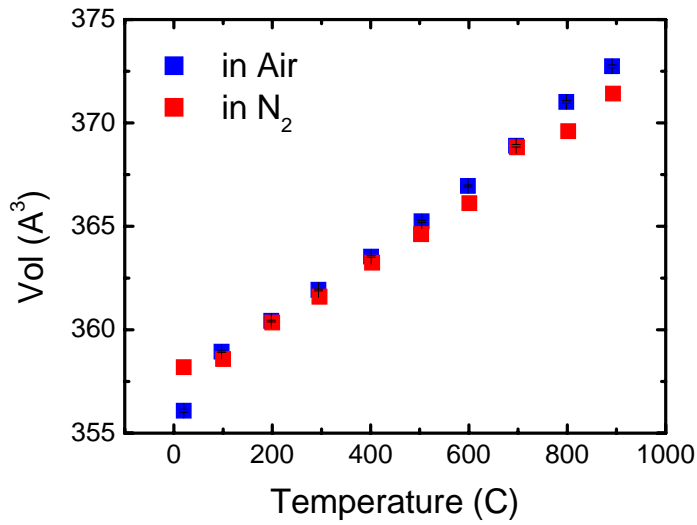
Fig. 3. Unit cell volume as a function of temperature for LSFT in air and N_2.
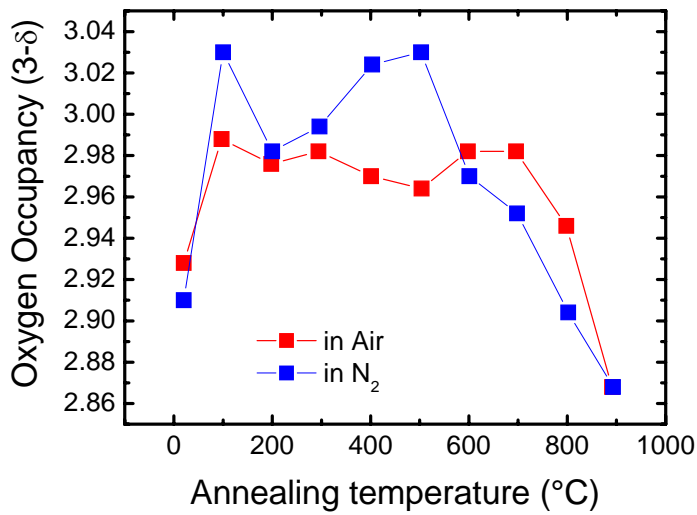
Fig. 4. Oxygen occupancy (3-δ) as a function of measuring temperature for LSFT in air and N_2.

TASK 2: **Determine material mechanical properties under conditions of high temperature and reactive atmosphere**

Prof. Sukumar Bandopadhyay and Dr. Nagendra Nagabhushana
University of Alaska Fairbanks

In this quarter, studies were continued on dense OTM bar samples received from Praxair. A new fixture was designed to provide sharp pre-crack and stable crack growth studies were performed. X-ray data was refined for deriving lattice parameters and TG-DTA analysis were performed on post-fracture specimens.

Experimental:

Design of Bridge-cracking fixture:

In the previous studies on evaluating fracture toughness there was the question of obtaining

Fig. 5. Pre-cracking fixture and stable crack growth in indented dense OTM samples.
a) Vickers indent along the center line; b) Bridge Cracking fixture; c) 4-Point failure at the pre-cracked point; d) Stereo micrograph indicating stable crack growth and fast fracture.

stable crack growth requisite for fracture mechanical calculations. Studies on bars samples with an Vickers indent or from a sharp notch were inconclusive due to absence of stable crack growth features. In the present quarter, a pre-cracking fixture ter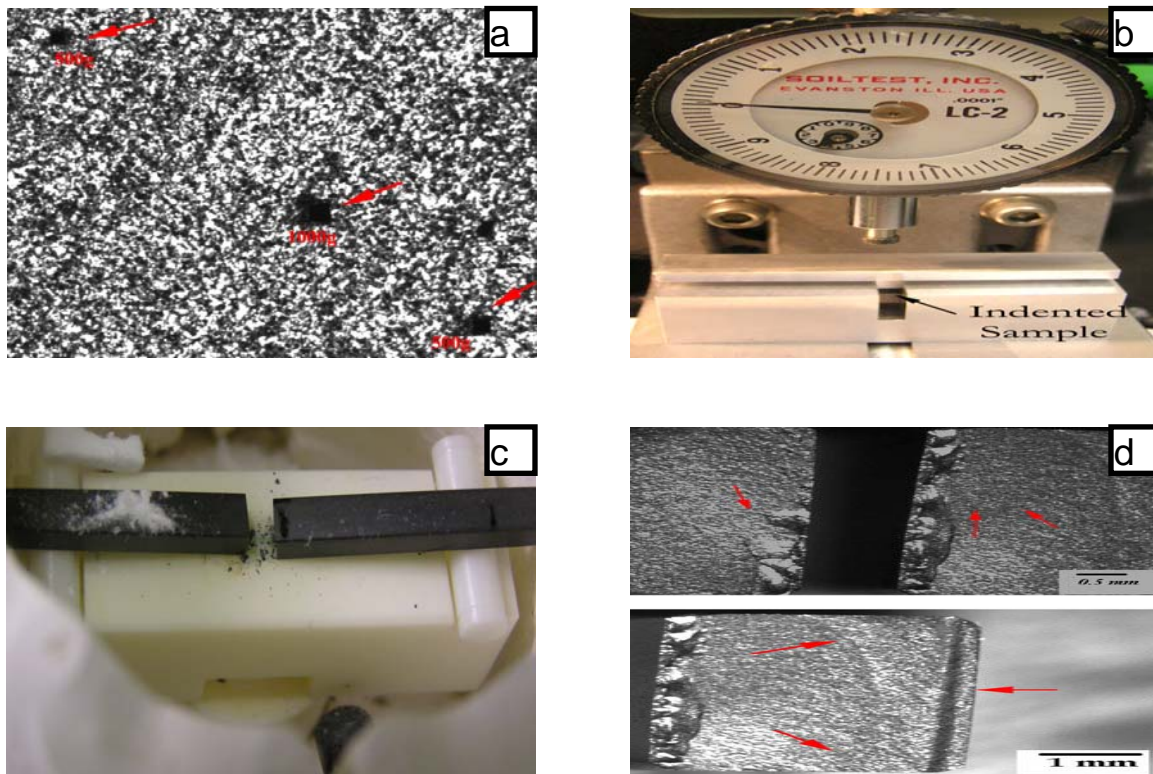med as "Bridge-compression technique" was fabricated. The rationale behind the technique is the application of small and controlled tensile forces on a Vickers indent to start a stable pre-crack. Upon release of the load, the pre-crack is arrested and the cracked sample is loaded in the 4-point flexure testing fixture.

As shown in Fig. 5a, Vickers indents were placed along the center line of the polished dense OTM bar sample. Vickers indent at the center of the line was with a 9.8 N load and the indents with a lower load (4.9N) were placed at a distance of 0.5mm from the indent at the center. The indented sample was loaded into the bridge fixture (Fig. 5b) such that the indents were on the tensile surface. The pre-load was applied and released through the top rod for a "n" number of times to ensure a uniform pre-crack from the indents. The pre-cracked specimens were loaded into the 4-point flexure and the tested at room temperature. As shown in Fig. 5c, the indented flexure bar did fail at the pre-cracked point and stereo microscope image (Fig. 5d) clearly indicates an indented region, a regime of slow and stable crack growth, fast fracture and compression curl in the tested sample. This result is indicative of a "good-test run" and since the method is very simple will also be used on samples to be tested in the environmental conditions (temp, pressure and chemical environment).
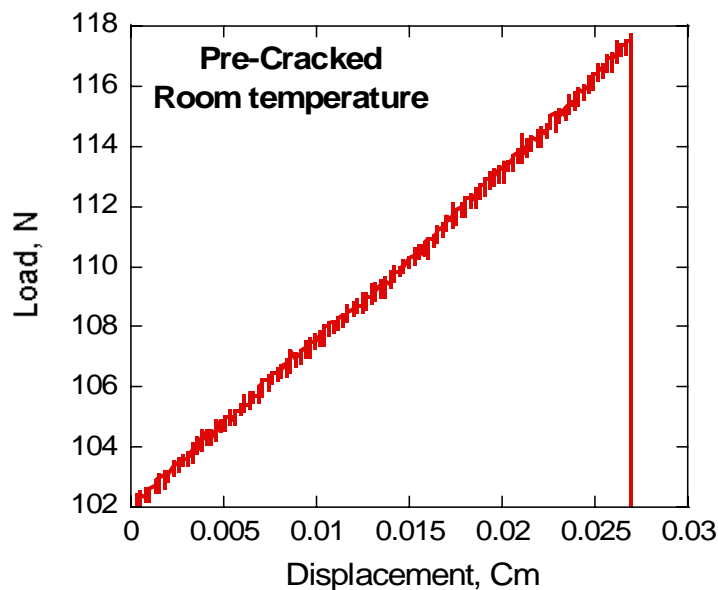

Fig. 6   OTM bar loaded to fracture after pre-cracking by Bridge-Compression technique.

Refinement of X-ray data:

In understanding the decomposition process in the dense OTM material after exposure to a combination of stress and environment, it is very important to refine the raw X-ray data to define the crystal parameters. In the previous report, the raw X-ray data were presented and several of the key peaks were indexed (by PowderX program) to structures arising from transition of the parent perovskite to related structures of brownmillerite and Aurivilius phases.

In the present quarter, the major peaks from the XRD data were selected and refined by Fullprof Code. The major peaks (2θ =22.94, 32.5, 39.91, 46.25, 52.56, 57.32, 67.69 and 77.17) were chosen based on the literature available and indexed to the cubic structure of the LSFCO material. The results of the refinement are plotted in Figure 7,8 and 9 respectively and the resulting lattice parameters listed in Table 3

3 – Exposed to N₂/Air, 1000C
2 – Exposed to Air, 1000C
1 – As Received

Fig. 7. Refinement of OTM material in as received and as exposed to air and N₂/air at 1000°C. Insets b and c, indicate the observed shift in 2θ values

3 – Fractured in N_2/Air, 1000C
2 – Fractured in Air, RT
1 – As Received

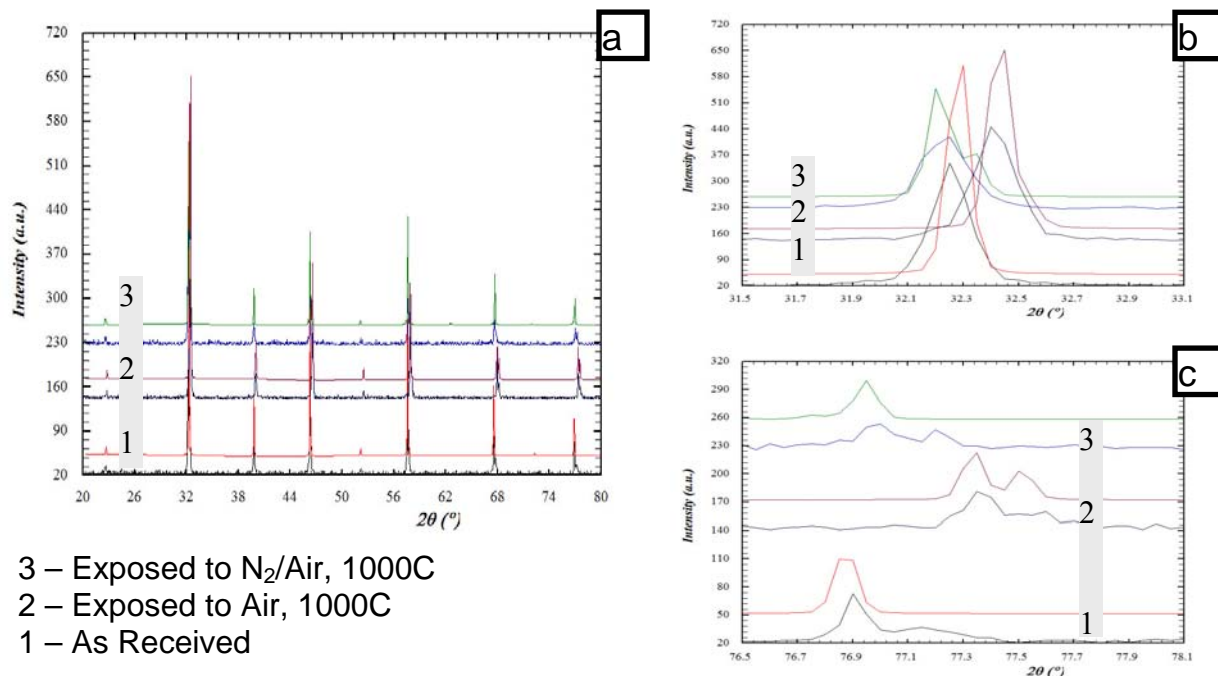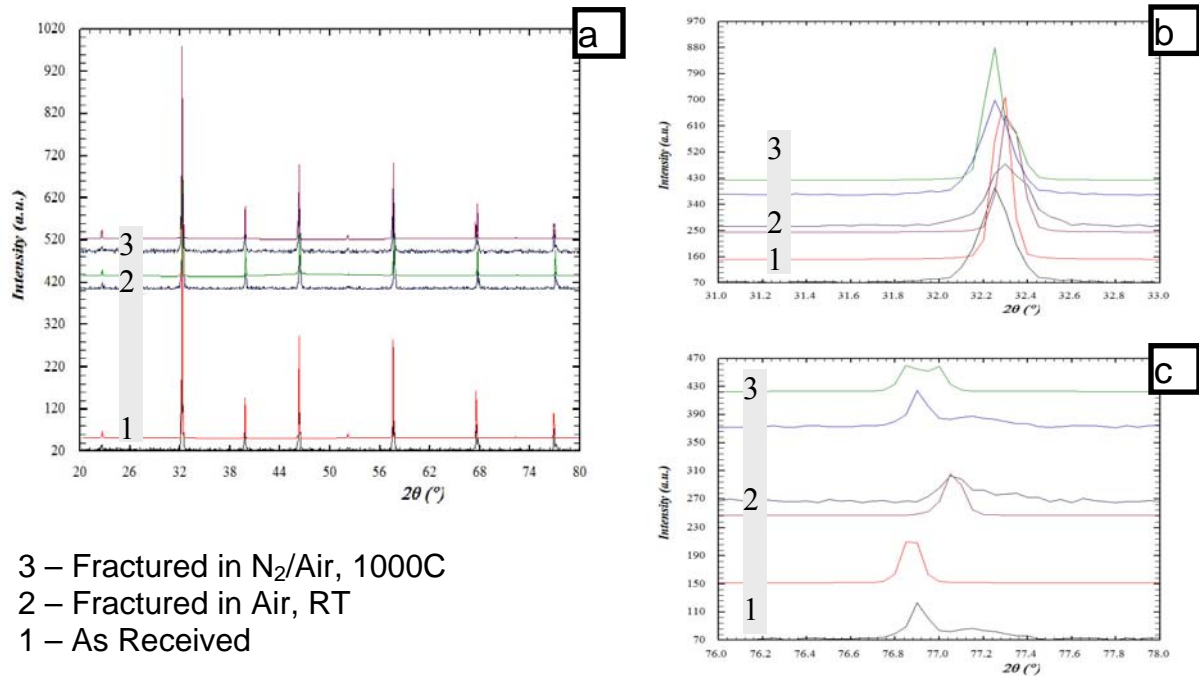Fig. 8. Refinement of OTM material in as received and fractured in air (RT) and N_2/air at 1000°C. Insets b and c, indicate the observed shift in 2θ values

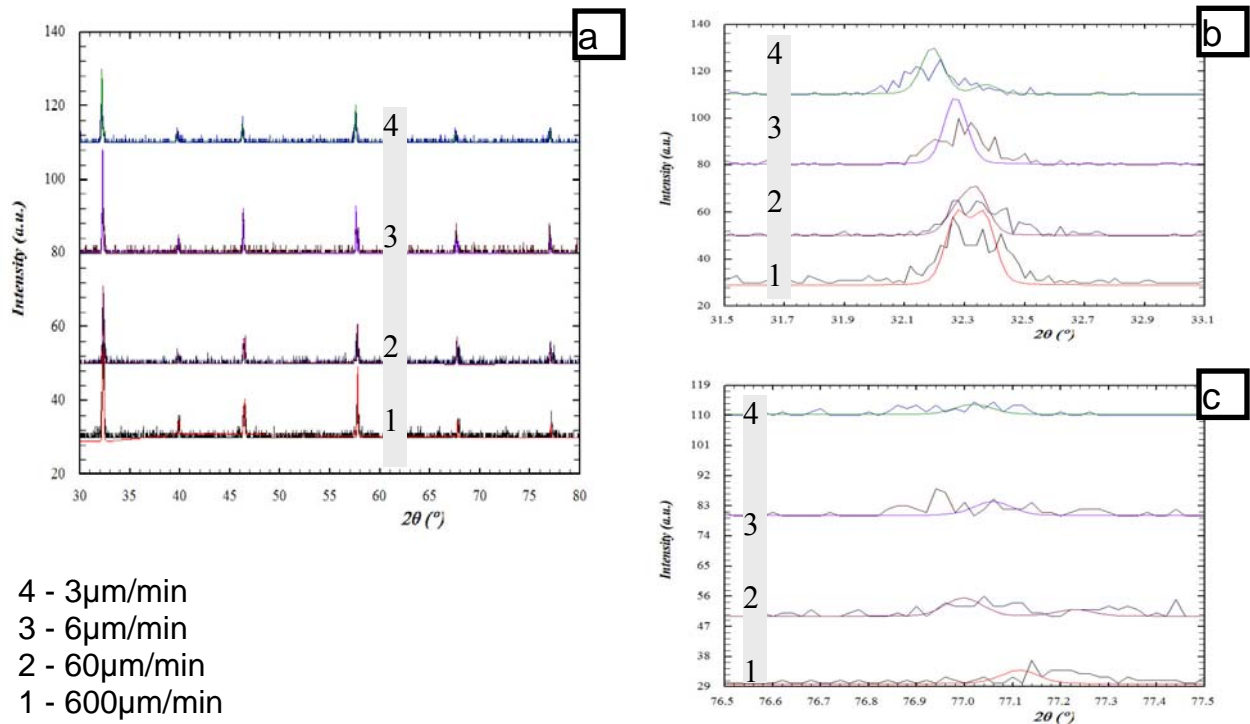
4 - 3μm/min
3 - 6μm/min
2 - 60μm/min
1 - 600μm/min

Fig. 9. Refinement of OTM material fractured in N_2/air at 1000°C at different stressing rates. Insets b and c, indicate the observed decomposition of the major peak and shift in 2θ values

14

Table 3.   Crystal Symmetry and lattice parameters obtained from refinement of XRD data.

Condition	Symmetry	a_c	b	c	$\alpha=\beta=\gamma$
As received	Pm3m	3.9104	3.9104	3.9104	90
Air exposed (1000ºC)	Pmmm	3.8991 (~a_c)	2.758 $b \sim a_c/\sqrt{2}$	2.7497 $c \sim a_c/\sqrt{2}$	90
N_2/Air exposed (1000ºC)	Pmmm	3.9362 (~a_c)	3.9174 (~a_c)	2.7634 $c \sim a_c/\sqrt{2}$	90
Fracture, RT	Pmmm	3.9134 (~a_c)	3.9085 (~a_c)	2.7647 $c \sim a_c/\sqrt{2}$	90
Fracture N_2/Air, (1000ºC)	Pmmm	3.9294 (~a_c)	3.9175 (~a_c)	2.7656 $c \sim a_c/\sqrt{2}$	90
Fracture N_2/Air, 600μm/min	Pmmm	3.9340 (~a_c)	3.9052 (~a_c)	2.7640 $c \sim a_c/\sqrt{2}$	90
Fracture N_2/Air, 60μm/min	Pmmm	3.9278 (~a_c)	3.9033 (~a_c)	2.7606 $c \sim a_c/\sqrt{2}$	90
Fracture N_2/Air, 6μm/min	Pmmm	3.9233 (~a_c)	2.7783 $b \sim a_c/\sqrt{2}$	2.7634 $c \sim a_c/\sqrt{2}$	90
Fracture N_2/Air, 3μm/min	Pmmm	3.9155 (~a_c)	2.7385 $b \sim a_c/\sqrt{2}$	2.7719 $c \sim a_c/\sqrt{2}$	90

The results from the refinement indicate that the parent perovskite with a primitive cubic perovskite structure (a=b=c = 3.9104Aº) undergoes a slight distortion to orthorhombic structure (Pmmm) with reduced crystal symmetry. Although slight changes are observed in the a axis, the distortion is primarily in the c and b axes. Interestingly, samples tested under stress and environment showed increasing distortion with decreasing stress rates. However, although the major peaks were refined, the broader reflections and splitting of several peaks indicate the possible presence of secondary phases etc. further refinement of the data will be done considering various phase composition determined by XRD.

Although, the XRD analysis indicated phase instability and decomposition of the parent perovskite upon exposure to the environment and stressing rates, the possibility of vacancy ordering and structure change in micro-domains need to be examined. For this studies were done in a TGA-DTA (Perkin Elmer Instruments) to obtain relevant information on endothermic and exothermic processes corresponding to different oxygen desorption processes and structural

changes for ex:: vacancy order-disorder transitions and reversible structural stability of the materials.

Initial TGA studies were done by retaining the thermal history of the materials tested. For these the tested bar samples were sectioned and heated in N_2 up to 1000ºC with a equilibration time of 1 hr. As shown in Fig.10, the weight loss and the DTA signal were monitored for further analysis.
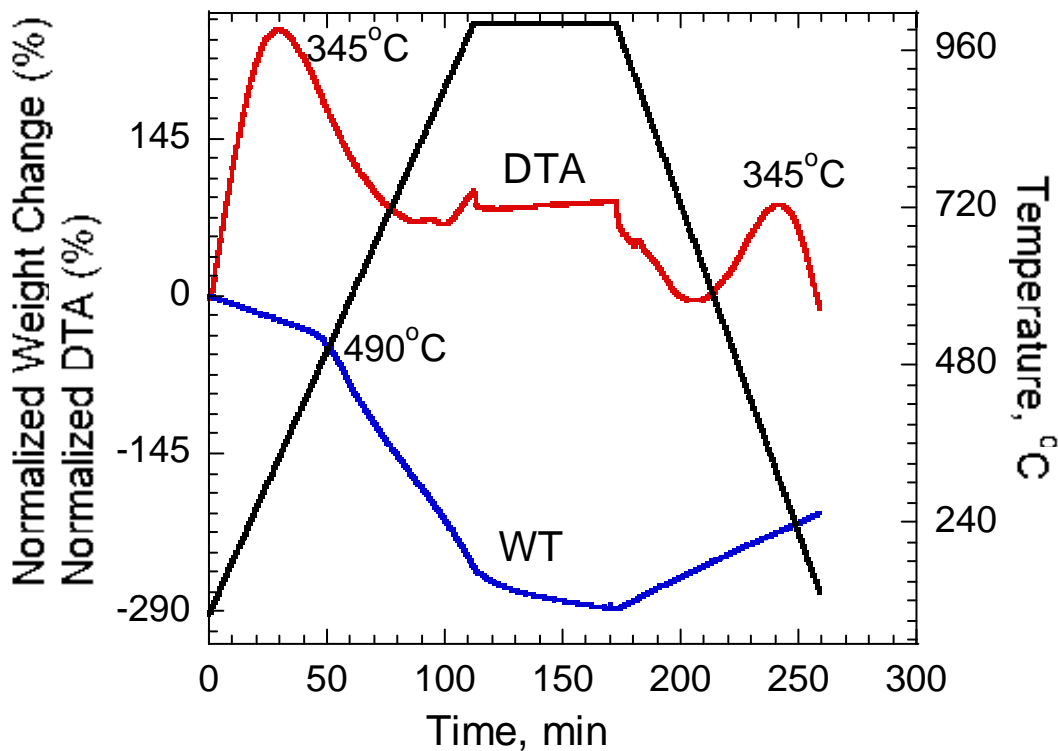
Fig 10: Weight change, DTA and temperature data as a function of time.

As shown in Fig. 11 and Table 4, post- fracture thermal analysis studies on the sample indicate significant changes in weight and DTA signal. The As-received sample indicate a continuous change in weight with increasing temperature till around 235ºC and thereafter a plateau wherein no change in weight was observed. A second weight loss was observed around 850ºC. On the other hand, sample exposed to an environment of N_2 changing to air at 1000ºC and samples fractured in the same environment indicated a drastic weight loss at higher temperature. The onset temperature for the drastic weight loss varied depending on the stress history [Table 4].
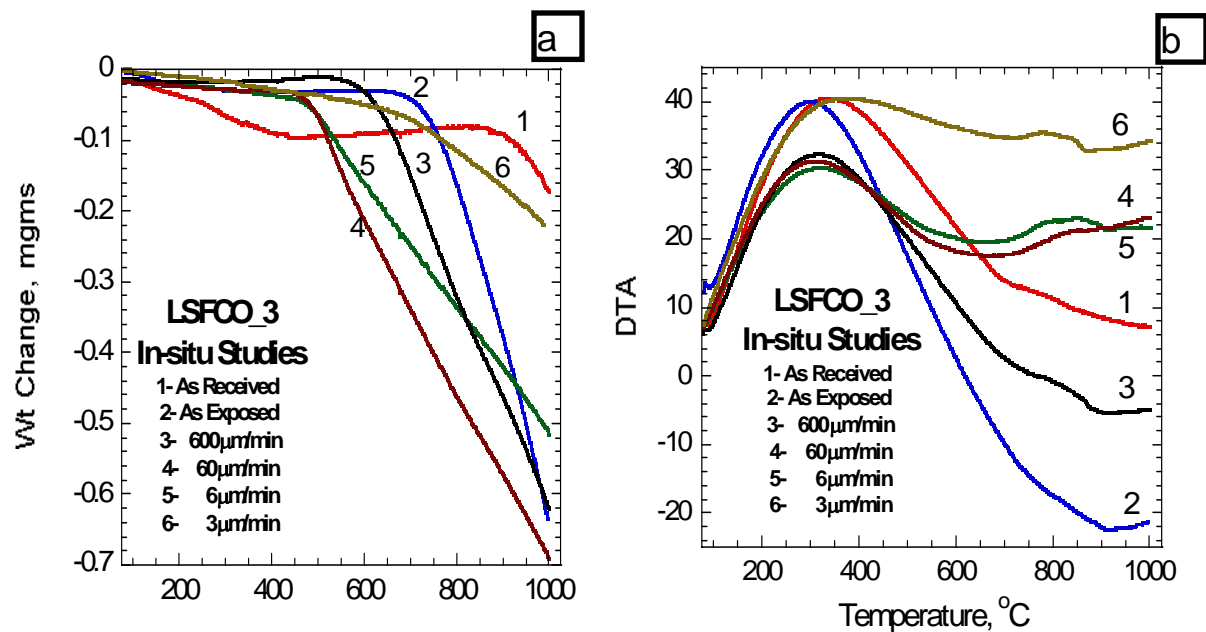
Fig. 11.   Post-fracture thermal analysis of LSFCO-3 OTM material.

The DTA signal (Fig 11b) also indicated changes and depending on the sample history, an highly exothermic peak were observed in the temperature range of 310- 350ºC. A second peak prominent in samples fractured in the environment was also observed in the temperature region of 775-800ºC. This peak was of low intensity and was masked in the as-received sample

Table 4:   Thermal analysis of LSFCO-2 samples.

	Wt Loss	Wt loss	DTA (peak 1)	DTA (peak 2)
As received	235ºC	850ºC	336ºC	801ºC
Exposure N_2/Air 1000C		680ºC	300ºC	805ºC
600µm/min N_2/Air 1000C		542ºC	311ºC	777ºC
60µm/min N_2/Air 1000C		455ºC	316ºC	802ºC
6µm/min N_2/Air 1000C		450ºC	333ºC	847ºC
3µm/min N_2/Air 1000C		670ºC	348ºC	777ºC

The stoichiometry (δ) of the samples were determined from weight change measurements and calculated as:

$$\delta = \delta_0 + \frac{(W_i - W_s)/M_o}{W_i/M_{w,0}}$$

W_i = initial weight
W_s = equilibrium Weight
M_o = atomic weight of oxygen
$M_{w,0}$ = molecular weight of sample
δ_o = 0.2379 at 800°C in 10^{-4}

δ_o for the calculation were obtained from Prof. Jacobson's work on $La_{0.2}Sr_{0.8}Fe_{0.8}Cr_{0.2}O_{3-x}$ as apart of the present program
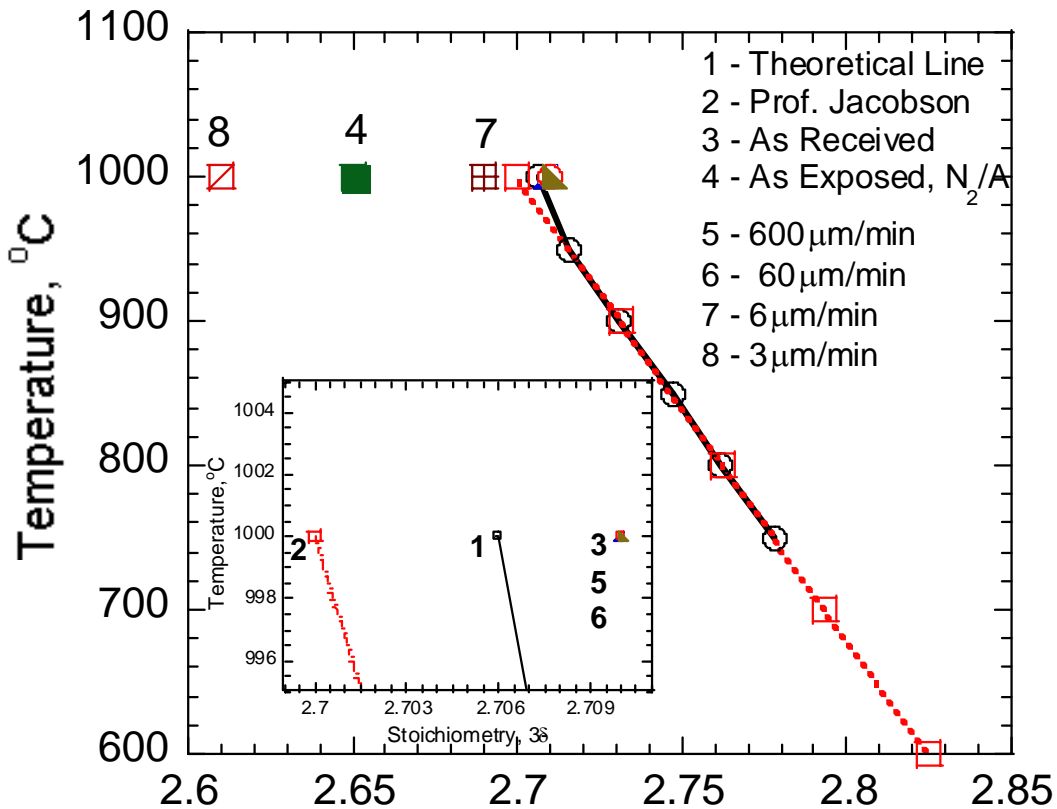
Fig. 12. Stoichiometry (3-δ) of the fractured samples calculated from weight change measurements in a TGA

The results indicate that there is a perceptible change in stoichiometry of the fractured OTM membrane as compared to related studies on non-fractured samples. However, based on the discussion with the group at the project meeting further tests such as removing the thermal and applied stress history by annealing are planned to confirm the results.

Task 3:   Measurement of Surface Activation/Reaction rates in Ion
Transport Membranes using Isotope Tracer and Transient Kinetic Techniques.

Prof. Alan Jacobson, University of Houston/University of Toronto

EXPERIMENTAL

The experimental techniques used to generate the results reported here have been described in previous quarterly reports

RESULTS AND DISCUSSION

Conductivity and Thermodynamic Studies

So far, we investigated the thermal and chemical expansion of the sample only at high pO_2 region ($\sim 1 \times 10^{-4} \leq pO_2 \leq 0.21$ atm). At this point, it is necessary to study the length variations at further reduced pO_2 environment. Using the metal-metal oxide solid buffer is one way to obtain the lower pO_2 condition but with this method is not easy to maintain a constant pO_2 value for a long time. Instead in this experiment, the lower pO_2 values of less than $\sim 10^{-10}$ atm can be obtained by using 5% H_2/N_2 (1~3 ml/min), CO_2 (50 ml/min) and argon (100 ml/min). Mass flow controllers were used to control the proper amount of gas supplied to the dilatometric furnace.

Fig. 13(a) shows the chemical expansion of the sample bar as a function of time at 850 °C. Purified air was used as the gas until the temperature reached at 850 °C and the thermal expansion of the sample was measured. After the length reached equilibrium in the isothermal region, the air was switched to a gas mixture. The emf output from a YSZ oxygen sensor was monitored every single minute throughout and used to calculate the pO_2 .The chemical expansion data were obtained at one data point per minute. By using the mixed gas, 5% H_2/N_2, CO_2, and argon, the value of pO_2 can be lowered to $\sim 10^{-15}$ atm and a second equilibrium state appears. The length of the sample did not change for several hours. The oxygen partial pressure was increased again by cutting off the 5% H_2/N_2 gas until $pO_2 \sim 10^{-4}$ atm. At this stage, the pO_2 values increased very rapidly but the length of the sample changed only slowly. Finally, the gas was switched to air and the temperature was decreased. The thermal expansion determined in the course of heating shows good agreement with that of the decreasing temperature. Even though

the sample was in a reducing environment at high temperature for more than 16 hours, no evidence was found for any decomposition.

Fig. 13(b) displays the pressure dependence of the chemical expansion in both high to low and low to high pO_2 directions at 850 °C. The length of the sample expands abruptly in the range of pO_2 between 0.21 atm and $\sim 10^{-6}$ atm, shows a kink around $\sim 5 \times 10^{-6}$ atm, and expands slowly until the pO_2 reaches $\sim 10^{-15}$ atm. On increasing pO_2, the variation of the sample contraction occurred too slowly to keep up with the rate of change of the pO_2. When the pO_2 reached a constant value at $\sim 10^{-4}$ atm, the dL value approached to the dL value obtained in the high to low pO_2 direction. These trends appear in the same way by changing the gas to air. Reproducibility of the measurements in both directions will require a much slower rate of change of pO_2.

Fig. 14 shows the chemical expansion as a function of oxygen partial pressure for $La_{0.2}Sr_{0.8}Fe_{0.55}Ti_{0.45}O_{3-\delta}$ at $800 \leq T \leq 950$ °C and at $\sim 10^{-15} \leq pO_2 \leq 0.21$ atm. It also shows the comparison of the chemical expansion with the oxygen non-stoichiometry (δ) obtained by the solid-state coulometric titration. The lines indicate the coulometric titration results are consistent with the chemical expansion at $800 \sim 850$ °C. This suggests that the degree of chemical expansion is controlled by the concentration of oxygen ion vacancies. However, a significant difference is observed in the two curves measured at 950 °C and 1000 °C. The changes in slopes appear at all temperatures and move to lower pO_2 as the temperature increased. The origin of these changes in slopes is not yet but may reflect cation rearrangements.

The kinks are very distinct at the plot of normalized change of length (dL) as a function of pO_2 as shown in Fig. 15(a). Chemical expansion data are normalized by using the temperature-dependent dilatometric data reported previously. Fig. 15(b) presents the plot of normalized dL vs. oxygen non-stoichiometry (δ). According to the comparison of dL and δ as a function of pO_2 in Fig. 16, a linear relation is expected. The lines at 800 and 850 °C are almost linear but those at 900 and 950 °C are not. These data show an unexpected behavior near the stoichiometric composition ($\delta = 0.175$) suggesting the possibility of a phase transition.
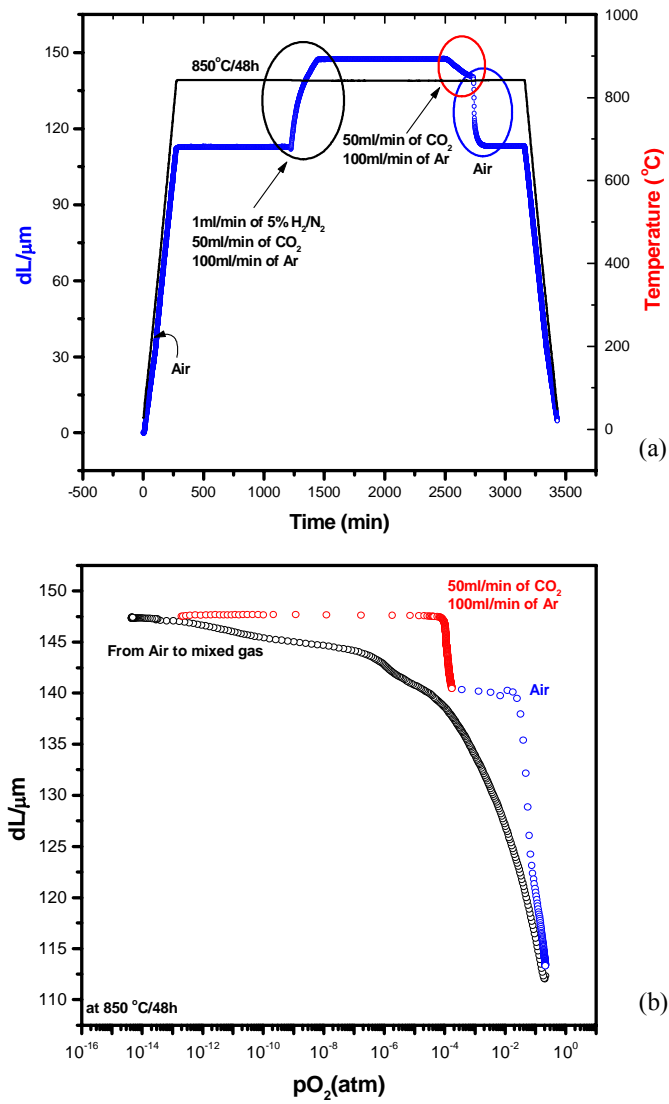
Fig. 13.   (a) Chemical expansion data for $La_{0.2}Sr_{0.8}Fe_{0.55}Ti_{0.65}O_{3-x}$ vs. time; (b) vs. pO_2.
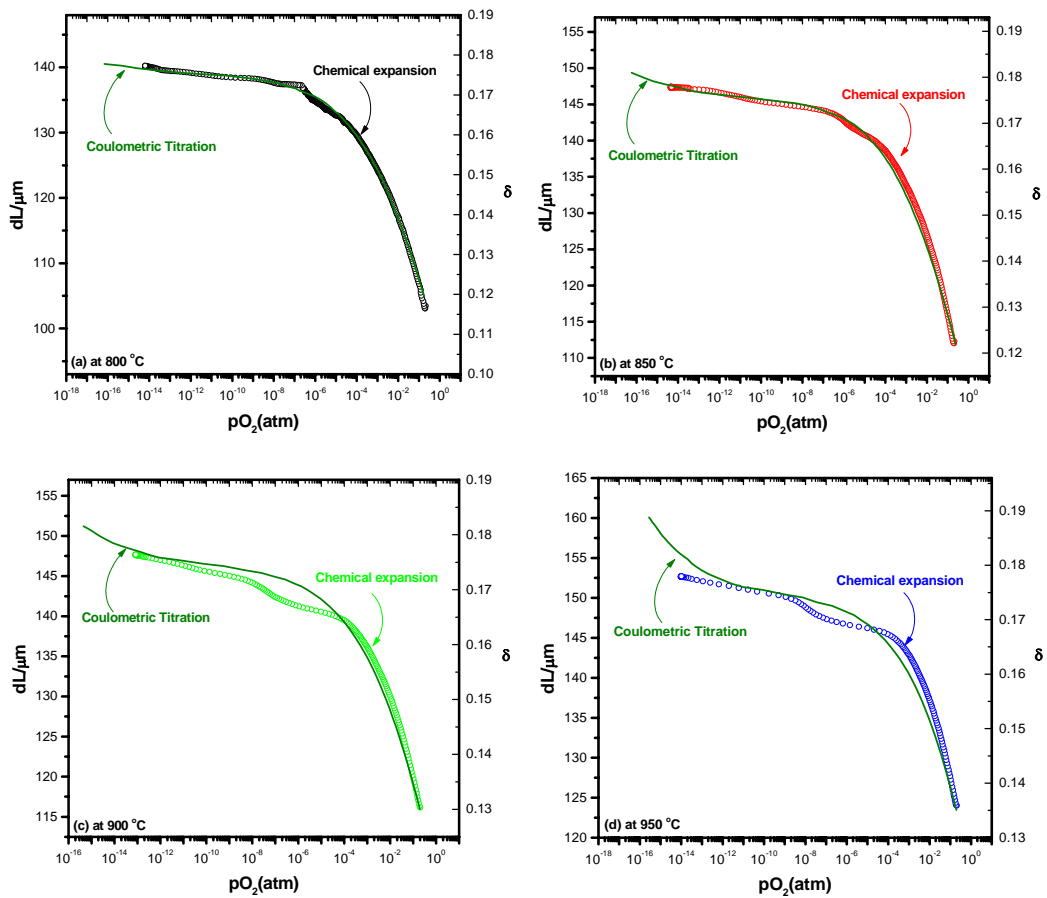
Fig. 14.   pO$_2$ dependence of the chemical expansion of La$_{0.2}$Sr$_{0.8}$Fe$_{0.55}$Ti$_{0.65}$O$_{3-x}$ (a) 800 °C, (b) 850 °C, (c) 900 °C, (d) 950 °C. The continuous lies are the corresponding changes in non-stoichiometry.

Fig. 15.   (a) pO$_2$ dependence of the chemical expansion of La$_{0.2}$Sr$_{0.8}$Fe$_{0.55}$Ti$_{0.65}$O$_{3-x}$ (b) dependence of the chemical expansion on stoichiometry.

plot of normalized dL vs. oxygen non-stoichiometry (δ). According to the comparison of dL and δ as a function of pO$_2$ in Fig. 16, a linear relation is expected. The lines at 800 and 850 °C are almost linear but those at 900 and 950 °C are not. These data show an unexpected behavior near the stoichiometric composition (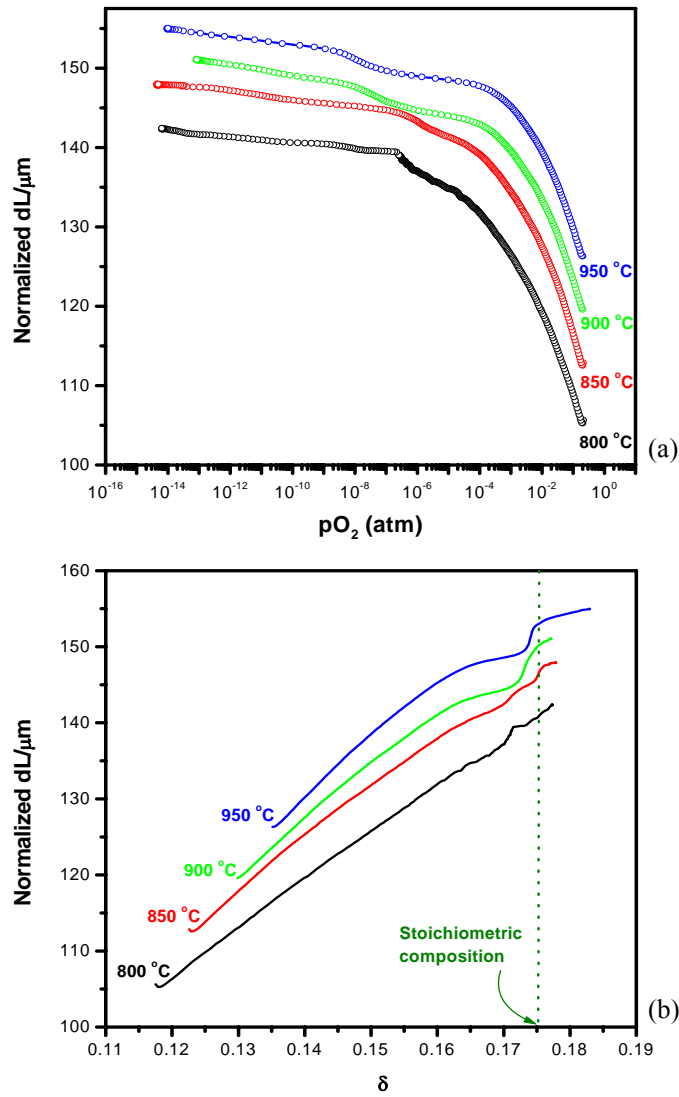δ = 0.175) suggesting the possibility of a phase transition. Therefore, samples were quenched from 900 °C and at pO$_2 \sim 1 \times 10^{-7}$ atm and 8×10^{-14} atm. The X-ray powder diffraction data (Scintag, XDS 2000) for quenched and non-quenched samples are shown in Figure 4. No evidence of a phase transition is observed in the XRD powder patterns. Also, after the whole thermal and chemical expansion sequence of measurements, the same

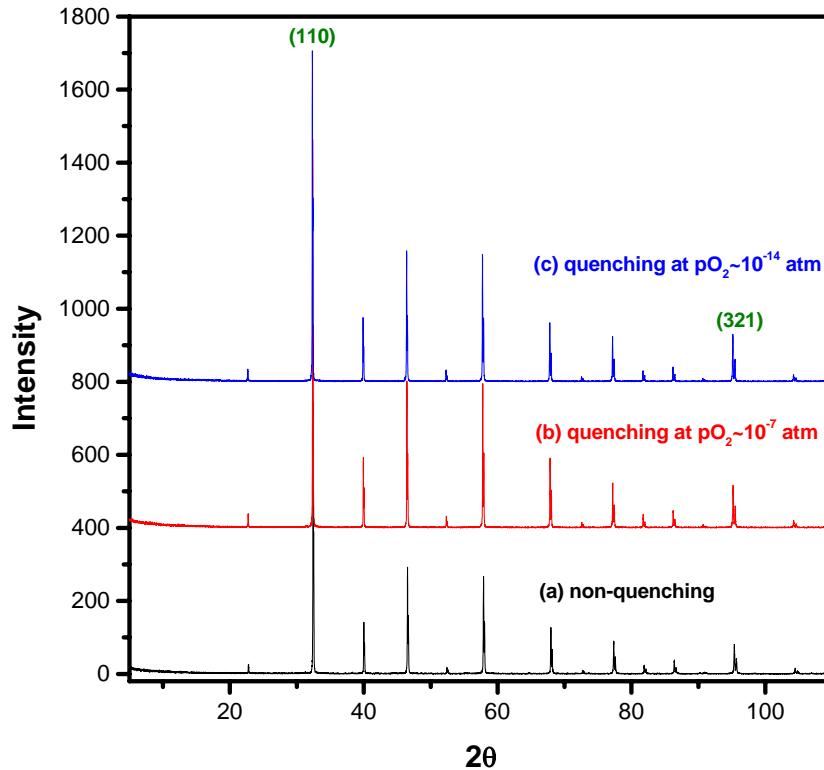temperature-dependent dilatometry data is observed as at the beginning.

Fig. 16. X-ray powder diffraction patterns of $La_{0.2}Sr_{0.8}Fe_{0.55}Ti_{0.65}O_{3-x}$ (a) quenched; (b) quenched from 900 °C and ~ 10^{-7} atm; (c) 900 °C and ~8×10^{-14} atm;

University of Toronto

Isotope Transient Studies at Steady State

Our last report described the end of experiments on $La_{0.6}Sr_{0.4}Co_{0.2}Fe_{0.8}O_{3-\delta}$ (LSCF-6428) and a brief summary of findings on a new membrane of $La_{0.2}Sr_{0.8}Cr_{0.2}Fe_{0.8}O_{3-\delta}$ (LSCrF-2828). During the past quarter we have done the following:

LSCF-6428 study: We are continuing the analysis of data from the LSCF-6428 study. For the quenched membrane data, we have reanalyzed regions of the quenched membrane with better resolution and signal/noise. We have used recently written data manipulation codes to allow us to retrieve isotope profiles from the SIMS data obtained on the tubular membrane geometry.

LSCrF-2828 studies under air separation mode: A series of isotope transients under air separation mode (small gradient) were completed on the membrane of LSCrF-2828 at 900°C. As

previously described, the reversibility of oxygen activation at the air side can be obtained by observing the exchange of oxygen from the solid into the air after the administration of the isotope labeled pulse. A reverse flux will introduce [18]O isotope into the air, now with natural abundance, from the newly labeled solid. This method was described in previous reports. Figures 5 and 6 shows the results and model fits.
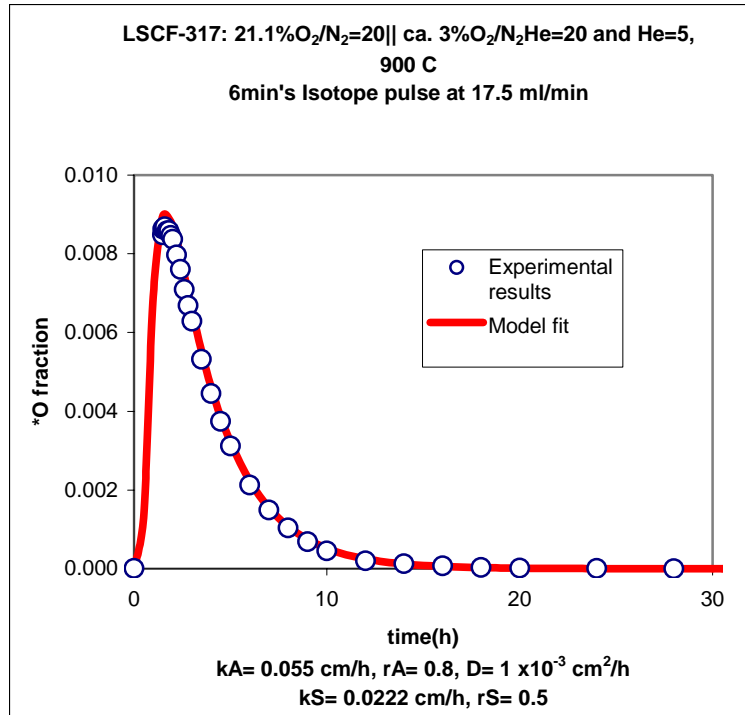

Fig. 17.　　Isotope transient in the delivery side of an LSCrF- 2828 membrane

LSCF-317: Oxygen-rich side
21.1%O2/N2=20|| ca. 3%O2/N2He=20 and He=5, 900 C
6min's Isotope pulse at 17.5 ml/min

time(h)
kA= 0.055 cm/h, rA= 0.8, D= 1 x10-3 cm2/h
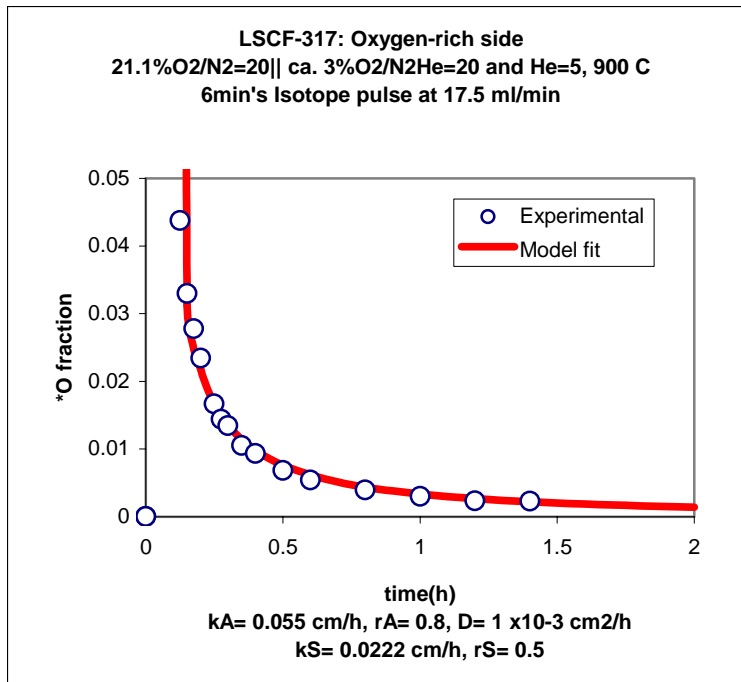kS= 0.0222 cm/h, rS= 0.5

Fig. 18.   Isotope transient in the oxygen on the air side of an LSCrF-2828 membrane.
Under these conditions, the molecular oxygen flux was 0.23 sccm.

LSCrF-2828 studies under syn gas generation mode:

Low pO_2 atmospheres based on with CO - CO_2 mixtures have also been admitted to the delivery side of the LSCrF-2828 membrane to produce the gradients which exist under syngas generation conditions. The CO - CO_2 mixtures have normal isotopic [18]O abundances. The evolution of [18]O on the delivery side in these experiments after an [18]O pulse on the air side reveals a wealth of information about the oxygen transport processes under steady operation. Figure 19 indicates the three oxygen transport processes which contribute to the isotope transient on the delivery site. These are (from top to bottom on the right side of the figure): (1) the evolution of molecular oxygen as in air separation mode, (2) oxygen delivery as CO is oxidized to CO_2 and (3) the rapid oxygen exchange between CO_2 and the surface. The oxygen evolution reaction, (1), by necessity produces oxygen molecules with the surface isotopic composition. Further exchange with the surface subsequent to formation will not affect the isotopic composition. The rapid exchange between CO_2 and the surface also guarantees that the isotopic fraction in CO_2 is that of the surface, regardless of the fact that unlabelled CO_2 is fed to this side of the membrane. If this CO oxidation reaction is partly reversible, i.e. CO_2 reduction takes place, the surface label will appear in CO. If CO_2

formation is irreversible, then no ^{18}O will appear in CO. If the redox reaction is very rapid, then CO and CO_2 will have the same isotope fractions.
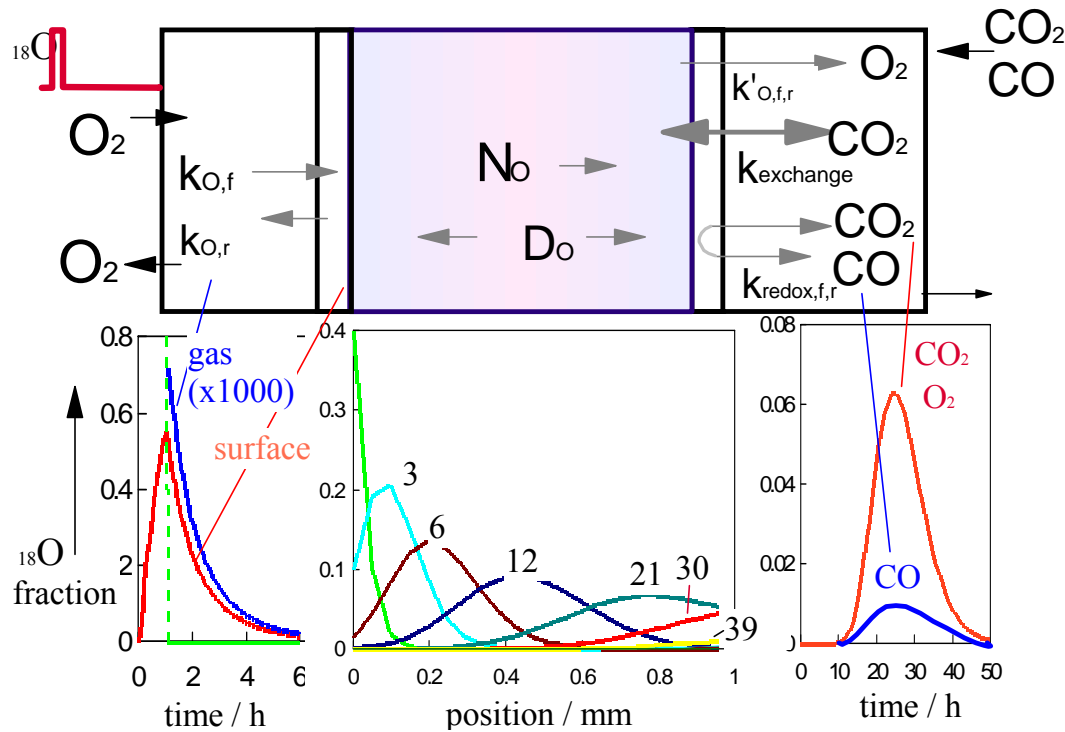

Fig. 19.   Schematic of the isotope transient experiment on a membrane with CO-CO2 on the delivery side (upper portion of the figure). On the air (left) side, forward and reverse oxygen uptake is indicated by the arrows and the appropriate surface rate coefficient (f = forward, r = reverse). The right side shows the three processes described in the text. The lower portion of the figure shows the isotope response as a function of time in the gases on either side of the membrane as well as isotope profiles in the solid at various times during the transient.

Important qualitative information can be realized from the data from such experiments:

(1) If oxygen is evolved on the delivery side, then the oxygen activity of the delivery side surface must be equal to or higher than the oxygen partial pressure in the gas. Under these circumstances, the activity gradient across the membrane is relatively small and the flux should be correspondingly reduced, if bulk transport limitations are significant. Also under these conditions, by virtue of the relatively high oxidation state of the surface, the reverse of CO oxidation should be disfavored.

(2) If CO oxidation is rapid enough to draw the oxygen activity at the delivery surface down to lower values, then molecular formation should also be much more limited. Simultaneously, the flux should rise by comparison with case 91). If CO oxidation is

rapid enough to be largely reversible (and ^{18}O labeling of the CO is observed), then the oxygen potential at the delivery surface would be ~10^{-16} .and oxygen pressures higher than that should not form.

The experiments on LSCrF 2828 revealed both of these regimes as the inlet CO concentration and temperature was raised. Figure 20 shows the results of a high gradient case (900 C and high CO concentration fed to the delivery side). No molecular oxygen was observed under these conditions.
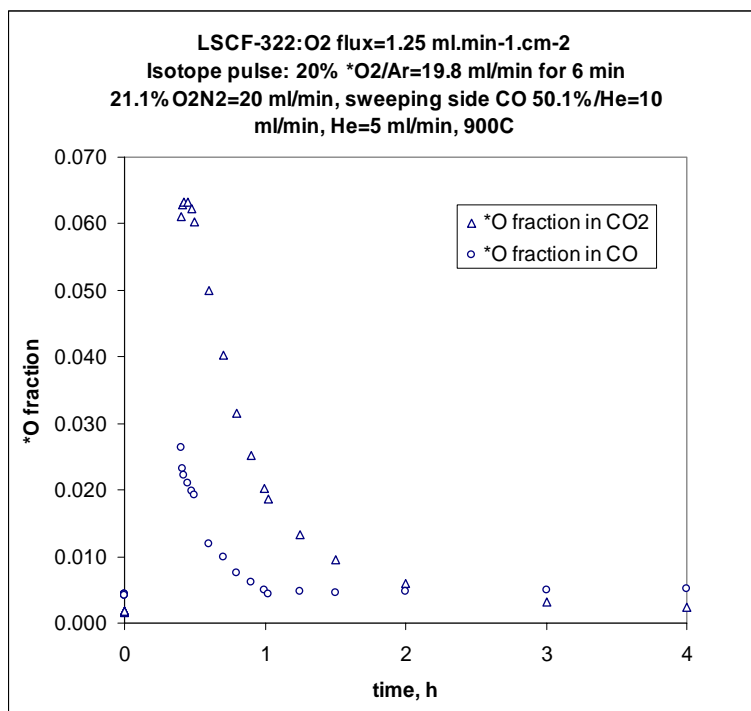

LSCF-322:O2 flux=1.25 ml.min-1.cm-2
Isotope pulse: 20% *O2/Ar=19.8 ml/min for 6 min
21.1%O2N2=20 ml/min, sweeping side CO 50.1%/He=10
ml/min, He=5 ml/min, 900C

Fig. 20.   Oxygen isotopic transient in both CO and CO_2 as a result of an ^{18}O isotopic pulse on the air side of the membrane.

Partial labeling of the CO on the delivery side indicates that that surface is functioning at a reduced state. The increased gradient across the membrane produces a 5-6 fold flux increase over the air separation conditions. Note the much faster response time in the transient arising from the higher flux. As a result of the larger activity gradient, the reversibility on the air side was also substantially reduced.

At low CO partial pressures (< 0.05 atm at 1173K), a mode was observed where oxygen recombination on the "fuel" side was competitive with CO oxidation. This was accompanied by a small oxygen potential gradient across the membrane, with the fuel side surface at a high oxygen potential, molecular oxygen in the "fuel" side gas and a low oxygen flux. Isotope transients showed that under these conditions, oxygen activation on the air side was largely reversible and CO oxidation on the "fuel" side was irreversible.

We have thus collected data at 1073K - 1173K under various conditions relevant to air and syngas production. The model derived numbers will be discussed in the next quarterly report.

Quench experiments

At the end of these experiments, the sample LSCrF 2828 membrane was quenched mid- transient as previously done for LSCF-6428. The initial profiles, obtained by a visiting student from Technical University, Munich, Stefan Gruber show a largely invariant radial profile as a function of azimuthal angle.

Dissemination: Two abstracts based on the work here have been submitted to the December MRS Meeting in Boston.

CONCLUSIONS

For a detailed analysis of the transport properties Ti doped LSF further studies are need to be by *In situ* neutron diffraction. Presently, the space group of R3c yields a better refinement than a cubic structure of Pm3m. The oxygen occupancy is observed to be nearly 3 in the region from room temperature to 700ºC, above which the occupancy decreased due to oxygen loss. These have implication on the thermal expansion of the crystal and needs to be correlated with physical measurements on Ti doped LSF.

Stable crack growth and fracture in LSFCO-OTM material can be achieved by using a bridge-compression technique for generating pre-cracks from indented flaws. Further studies need to be carried out in the next quarter to evaluate crack growth in reactive environment. TG-DTa studies by eliminating previous thermal or stress history are needed for better approximation of changes in stoichiometry.

The thermal and chemical expansion of $La_{0.2}Sr_{0.8}Fe_{0.55}Ti_{0.45}O_{3-\delta}$ were studied at $800 \leq T \leq 1000$ °C and at $\sim 1 \times 10^{-15} \leq pO_2 \leq 0.21$ atm. The thermal expansion coefficient of the sample was calculated from the dilatometric analysis in the temperature range between room temperature and 1200 °C in air. The results show a direct relation between the stoichiometry and chemical expansion and also show that titanium is effective at reducing the overall expansion. A series of isotope transients under air separation mode (small gradient) were completed on the membrane of LSCrF-2828 at 900°C. Low pO_2 atmospheres based on with CO - CO_2 mixtures have also been admitted to the delivery side of the LSCrF-2828 membrane to produce the gradients which exist under syngas generation conditions. The CO - CO_2 mixtures have normal isotopic ^{18}O abundances. The evolution of ^{18}O on the delivery side in these experiments after an ^{18}O pulse on the air side reveals a wealth of information about the oxygen transport processes relevant to membrane reactor design

REFERENCES

N/A

BIBLIOGRAPHY:

N/A

LISTS OF ACRONYMS AND ABBREVIATIONS:

OTM   Oxygen Transport Membrane

LSFCO   Lanthanum Strontium Iron Chromium Oxide ($La_{0.2}Sr_{0.8}Fe_{0.8}Cr_{0.2}O_{3-\delta}$)

LSF   Lanthanum Strontium Ferrite ($La_xSr_{1-x}FeO_{3-\delta}$)

LSCF   Lanthanum Strontium Cobalt Iron Oxide ($La_xSr_{1-x}Fe_{1-y}Co_yO_{3-\delta}$)

L2SF55T   Lanthanum Strontium Iron Titanium Oxide ($La_{0.2}Sr_{0.8}Fe_{0.55}Ti_{0.45}O_{3-\delta}$)